# A Study of Thermo-mechanically Processed High Stiffness NiTiCo Shape Memory Alloy

*R.M. Manjeri, D. Norwich, F. Sczerzenie, X. Huang, M. Long, and M. Ehrlinspiel*

This work investigates a vacuum induction melted-vacuum arc re-melted (VIM-VAR) and thermo-mechanically processed ternary NiTiCo shape memory alloy. The NiTiCo ingot was hot processed to 6.35-mm-diameter coiled wire. The coiled wire was subsequently cold drawn to a final wire diameter of 0.53 mm, with interpass anneals. The wires were shape set at 450 °C for 3.5 min. After electropolishing, the wires were subjected to microstructural, thermal, and mechanical characterization studies. Microstructural analysis was performed by transmission electron microscope (TEM), thermal analyses by differential scanning calorimeter (DSC), and bend-free recovery and mechanical testing by uniaxial tensile testing. TEM did not reveal Ni-rich precipitates—either at the grain boundary or in the grain interior. Energy dispersive x-ray spectroscopy showed a uniform distribution of Ni, Ti, and Co in the sample. The DSC results on the shape set wire showed a single-step transformation between the austenite and the R-phase, in the forward and reverse directions. Cyclic tensile tests of the shape set wire, processed under optimum conditions, showed minimum residual strain and a stable upper plateau stress. Further, the fatigue behavior of NiTi and NiTiCo alloys was studied by rotating beam testing. The results showed that the fatigue properties of NiTiCo, under zero mean strain, are equivalent to that of binary NiTi in the high-cycle and medium-cycle regimes, taking into account the higher stiffness of NiTiCo. The above analyses helped in establishing the processing-structure-property correlation in a VIM-VAR-melted NiTiCo shape memory alloy.

## 1. Introduction

The Nitinol-medical device industry has been trending toward reducing device size, while retaining or improving functional properties. This has led to renewed interest in NiTi-based ternary alloys with enhanced material properties. Of particular interest is the ternary NiTiCo system. Co additions to NiTi reduce the phase transformation temperatures, alter the phase transformation sequence, and affect the mechanical properties and the functional properties (Ref 1, 2). For example, when processed under similar conditions, NiTiCo is known to offer higher stiffness relative to binary NiTi. Several researchers have investigated the NiTiCo shape memory alloys in the past. Nakata et al. (Ref 3) found that Co substitutes preferentially for Ni, in the NiTi lattice irrespective of the stoichiometry. Kishi et al. (Ref 4, 5) studied the tensile, microstructural, and fatigue properties and found that the transformation characteristics of NiTiCo alloys are similar to binary NiTi alloys, and under select aging conditions, lenticular (Ni, Co)$_4$Ti$_3$ precipitates can be observed. Further, the precipitate size and the distance between them increased with increasing aging temperature/time. Hosoda et al. (Ref 1) studied the influence of composition on the phase transformation and observed that the phase transformation temperatures decreased with increasing Ni and Co content. The potential use of NiTiCo in medical devices has been explored by Fasching et al. (Ref 6). Huang et al. studied the corrosion behavior of NiTiCo (Ref 7). Lekston et al. (Ref 8) and Mohammad et al. (Ref 9) studied the thermo-mechanical processing of NiTiCo. They observed nano-crystalline microstructure upon cold working and annealing at temperatures as low as 400 °C. Despite the numerous studies cited above, there is still a need to understand the ternary NiTiCo alloy from a processing-structure-property correlation standpoint. This is because, the optimum thermo-mechanical processing conditions for a ternary NiTiCo system are different from a binary NiTi system and processing under non-optimum conditions can lead to significant deterioration in the functional properties—shape memory and superelasticity. Additionally, there is a need to understand the fatigue properties of NiTiCo vis-à-vis binary NiTi. Fatigue life is an important factor for evaluating the suitability of materials for product design. Such a comparison will improve our understanding of the advantages and limitations in the use of NiTiCo. The current work investigates a commercially available vacuum induction melted-vacuum arc re-melted (VIM-VAR) and thermo-mechanically processed NiTiCo shape memory alloy. Microstructural, thermal, and mechanical characterizations were undertaken to evaluate the material response to thermo-mechanical treatment. Further, rotary beam fatigue testing was done to compare the fatigue properties of binary NiTi and ternary NiTiCo alloys. The results from this study have potential implications toward understanding the optimum processing conditions and the use of NiTiCo shape memory alloys for numerous medical device applications.

**R.M. Manjeri, F. Sczerzenie,** and **M. Long**, SAES Smart Materials, New Hartford, NY; **X. Huang** and **M. Ehrlinspiel**, Memry Corporation, Bethel, CT and **D. Norwich**, Memry Corporation, Bethel, CT and Wytech Industries, Rahway, NJ. Contact e-mails: maddy_manjeri@saes-group.com and michael_ehrlinspiel@memry.com.

## 2. Material and Methods

The NiTiCo ingot material used in this study was VIM-VAR melted at SAES Smart Materials consistent with ASTM F 2063-12 (Ref 10), with the exception of the cobalt addition. The nominal composition, in wt.%, of the ingot is Ti-55.3Ni-1.3Co. Cobalt preferentially substitutes for Ni, in spite of the Ni-rich stoichiometry (Ref 1, 3). The VIM-VAR ingot was hot rolled to a coiled wire, 6.35 mm in diameter. The hot-rolled coiled wire was subsequently thermo-mechanically processed to yield a 0.53-mm-diameter wire. All the samples were drawn to approximately 45% cold work on the final material. Further, they were shape set straight at 450 °C for 3.5 min under identical conditions. After heat treatment, the parts were electropolished and passivated per ASTM A967-05 (Ref 11). Microstructural characterization was done using a Tecnai F30 transmission electron microscope (TEM). The TEM sample was prepared using a FEI200TEM focused ion beam station. Thermal analysis was done by differential scanning calorimeter (DSC) and by bend and free recovery (BFR). The DSC measurements were made on an Instrument Specialists Inc., DSC550 following ASTM F2004-05 protocol (Ref 12). The functional $A_f$ was measured on a Confirmd Shapetrack® ST0804TF tester following ASTM F2082-06 (Ref 13). Uniaxial tensile tests were performed on an Instron 5565 machine following ASTM F2516-07 (Ref 14), while the fatigue tests were performed on a custom built rotating beam fatigue tester (RBT). For more details on the test set-up and test conditions, the reader is referred to (Ref 15).

## 3. Results and Discussion

### 3.1 Thermal Analysis

The phase transformation temperatures were measured on the fully annealed hot-rolled coiled wire (6.35 mm) and the thermo-mechanically processed wire (0.53 mm). Figure 1 shows the DSC thermograms from both the samples. The coil specimen was fully annealed at 850 °C in vacuum for 30 min followed by air quench. The wire specimen was not subjected to any additional heat treatments, after shape setting. The fully annealed coil sample shows a single-step transformation from B2(austenite) to B19′(martensite), while the shape set wire shows a one-step transformation from B2(austenite) to R-phase. The R-phase transformation in NiTi and NiTi-based alloys has been studied extensively and a good summary of the results can be found in (Ref 2). In brief, the R-phase can be introduced by (i) optimized thermo-mechanical treatments such as annealing and aging, (ii) thermal and mechanical cycling, and (iii) compositional effects such as ternary alloying. Hosoda et al. (Ref 1) studied the influence of Co addition on NiTi alloys of varying stoichiometry in solution annealed samples. They observed the intermediate R-phase in alloys with relatively higher concentration of the ternary element. In Ti-55.3Ni-1.3Co, the R-phase transformation is brought forth by thermo-mechanical treatments and not by the mere addition of Co. This can be inferred from Fig. 1, where R-phase transformation is seen in the thermo-mechanically processed wire but not in the fully annealed coil. The R-phase↔B19′ transformation was not seen at temperatures as low as −150 °C, in the shape set wire.
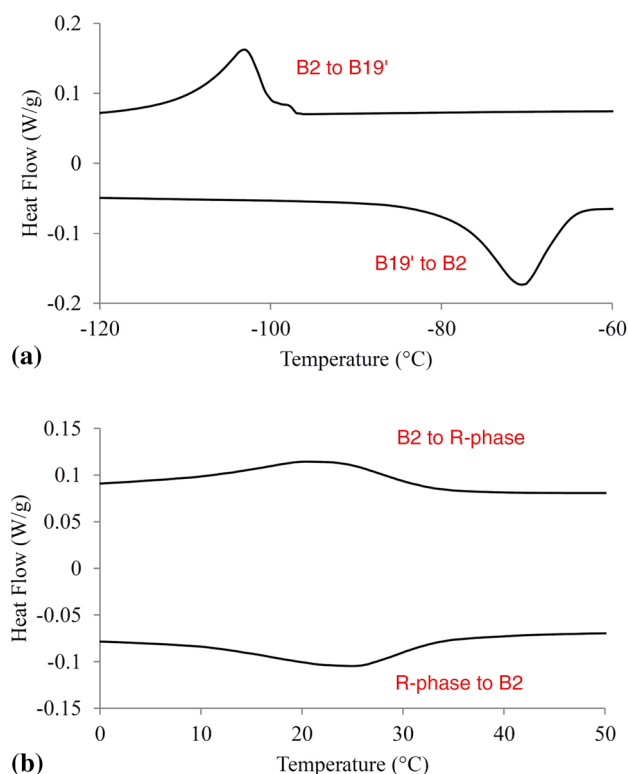


**Fig. 1** DSC thermograms from (a) hot-rolled coil (6.35 mm in diameter) and (b) cold-drawn and heat-treated re-drawn wire (0.5 mm in diameter)

The thermally induced R- and B19′ martensite phases in NiTi alloys are predominantly influenced by (i) the thermo-mechanical treatment and (ii) the grain size. Kishi et al. (Ref 4) studied the martensitic phase transformations in NiTiCo subjected to varying thermo-mechanical treatments. For the alloys heat treated at 350 °C, no B19′ phase was seen till temperatures as low as −150 °C. In the alloys aged at 450 °C, the B19′ phase transformation could be observed, only at longer aging times, both in the forward and reverse transformation. The grain size is also known to influence the thermally induced R- and B19′ phases. Recent studies on binary NiTi (Ref 16, 17) show that the thermally induced B19′ phase transformation is completely suppressed by reducing the grain size to < 60 nm. The suppression of the B19′ phase is attributed to the geometric and spatial constraints associated with the self-accommodation of the martensite. However, the stress-induced B19′ phase is not strongly influenced by the grain size. Ahadi et al. (Ref 17) have shown that the stress-induced B19′ phase is observed in grains as small as 10 nm. The absence of thermally induced B19′ phase in the 0.53-mm NiTiCo wire is due to the influence of grain size resulting from the thermo-mechanical treatment.

The functional $A_f$ of the shape set wire was measured using BFR test method. The BFR analysis was performed after cooling the sample to −60 °C, straining the sample by 2.5%, and subsequently heating the strained sample. The austenite finish ($A_f$) temperature, 18 °C, measured by the BFR is in disagreement with the DSC result, Fig. 2. Such a disparity in the measured transformation temperatures exists even in binary NiTi alloys processed under similar conditions. While it is outside the scope of this article to discuss the discrepancy

between DSC and BFR results, it is important to note that the BFR results demonstrate the austenitic phase is the stable room-temperature phase in the shape set wire. This was further confirmed by the tensile test results in section 3.3.
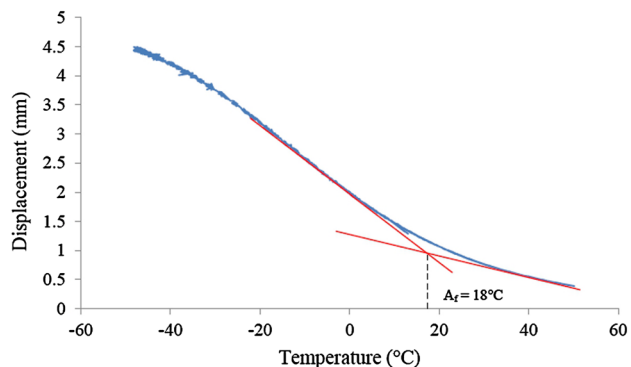


**Fig. 2** Functional $A_f$ measurement from bend and free recovery (BFR) test. The R-phase to B2 transformation is seen here upon re-heating

## 3.2 Microstructural Analysis

The microstructure of the shape set wire was studied by transmission electron microscopy (TEM). The TEM sample was prepared along the drawing direction. The bright field images are shown in Fig. 3. Figure 3(a) is a low-magnification view of the sample. The image shows the NiTiCo matrix and a TiC inclusion at the surface of the wire. Figure 3(b) shows the selected area diffraction pattern (SAD). The electron diffraction pattern confirms the stable phase at room temperature is B2 (austenite). No R-phase or B19′ phases were seen at room temperature. The diffraction pattern also indicates a nano-grain structure. The absence of additional reflections from secondary phases confirms the non-existence of Ni-rich precipitates. The SAD pattern indicates the ⟨110⟩ fiber texture in the thermo-mechanically processed sample. Figure 3(c) is a magnified view of a region within Fig. 3(a). The magnified image shows a nano-grain structured NiTiCo post the thermo-mechanical treatment. The grain size varied between 15 and 40 nm. The nano-grain microstructure is a consequence of heavy deformation followed by low-temperature heat treatment in the thermo-mechanical processing sequence. No Ni-rich precipitates are seen in the bright field image shown in Fig. 3(c). Microanalysis was carried in the scanning transmission electron microscope
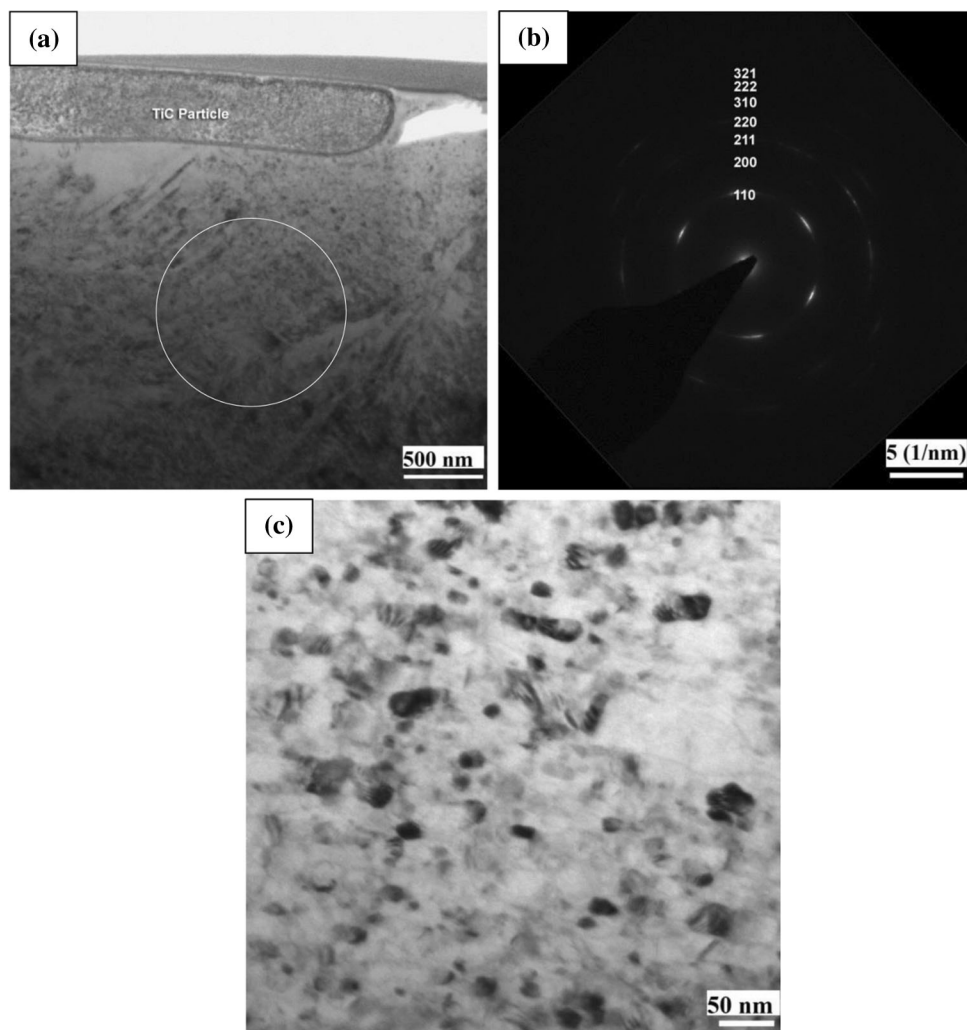


**Fig. 3** (a) Bright field TEM image at lower magnification (b) is the selected area electron diffraction pattern from the region indicated by the white circle and (c) nano-grains at a higher magnification. The SAD pattern confirms the absence of any secondary phase in the NiTiCo alloy
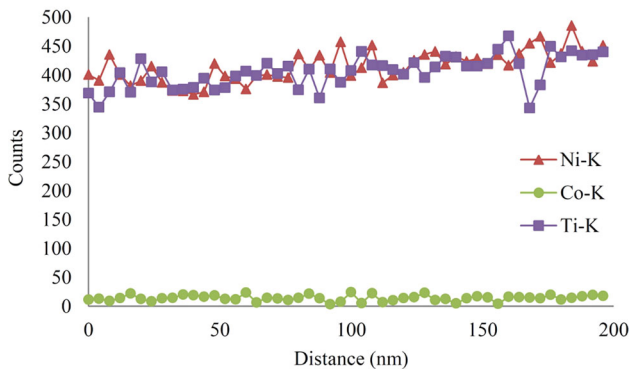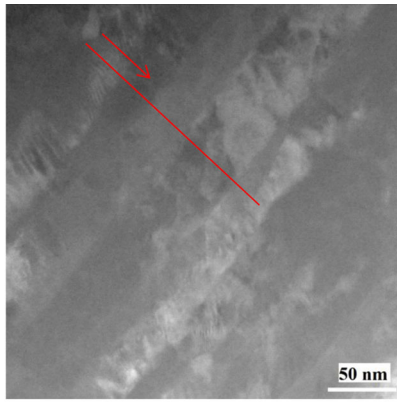
**Fig. 4** STEM-EDS analysis show the uniform distribution of Ni, Ti, and Co in the volume analyzed. The arrow indicates the direction in which the EDS analysis was performed and the red-line indicates the location where the analysis was carried

(STEM) mode by energy dispersive x-ray spectroscopy (EDS). The results indicate a uniform distribution of Ni, Ti, and Co in the volume analyzed. Thus, the STEM/EDS microanalysis confirms the absence of Ni-rich precipitates. The results are shown in Fig. 4. Ni-rich precipitates have been observed in NiTiCo alloys of different alloy formulations, in the past (Ref 4, 18). Kishi et al. (Ref 4) observed $Ni_4Ti_3$ lenticular precipitates in the NiTiCo heat treated at 350 and 450 °C. The heat treat time was varied between 30 and 3840 min. The precipitates grow in size with increasing aging temperature and longer aging time. In the present work, the TEM results show no evidence of precipitation of the Ni-rich phase. This is due to the influence of grain size from the relatively shorter heat treat time and lower heat treat temperature. Prokofiev et al. (Ref 19), Frotscher et al. (Ref 20), and Schaffer (Ref 21) made similar observations on their investigations of the nano-grained NiTi. Prokofiev et al. (Ref 19) did not observe Ni-rich precipitates in samples with grain size < 150 nm. They concluded that the geometrical constraints arising from the nano-grain microstructure resulted in the inability of the self-accommodation of the $Ni_4Ti_3$ precipitates, thereby suppressing the precipitation of the Ni-rich phase. Thus, the absence of precipitates in the thermomechanically processed wire is attributed to the nano-grain microstructure. Further, the low-temperature thermo-mechanical treatment suppresses the thermally induced B19′ phase and promotes the formation of R-phase, at relatively warmer temperatures. The suppression of the thermally induced B19′ phase is also associated with the nano-grain microstructure. As mentioned earlier, several studies (Ref 16, 17) have attributed

this inability to the geometric and spatial constraints associated with the self-accommodation of the variants formed in thermally induced martensite. Hence, only the B2 to R-phase transformation is seen in the DSC, till temperatures as low as −150 °C. However, it is important to re-iterate that the B19′ phase is observed, under the influence of external stress.

### 3.3 Mechanical Analysis

The downstream processing of NiTiCo uses identical equipment and process parameters as binary NiTi except for the final anneal temperature. NiTiCo is drawn using the same dies and die schedule as well as the same interpass anneal temperature as binary NiTi. The only difference in the processing of NiTiCo is that the final heat treat temperature is lower than the temperature used for binary NiTi. The heat treat time remains the same. This lowering of final anneal temperature holds true for all typical heat treatment methods used including tube furnace, salt pot, fluidized bed, and box furnace. The importance of the heat treat temperature, after the final pass, can be seen from Fig. 5 which shows the cyclic superelastic tensile properties of NiTiCo heat treated at three different conditions (a) 525 °C/3.5 min, (b) 450 °C/3.5 min, and (c) 450 °C/5 min. The sample heat treated at 525 °C shows an upper plateau stress (UPS) of 630 MPa and a residual strain of 0.23%. After 10 cycles, the corresponding values are 510 MPa and 0.6%, respectively. The lower heat treatment temperature for NiTiCo provides a more stable upper plateau and smaller residual strain. The UPS and the residual strain after 10 cycles for the sample heat treated at 450 °C for 3.5 min are 647 MPa and 0.25%, respectively. No significant difference is seen by changing the heat treat time from 3.5 to 5 min at 450 °C. This is shown in Fig. 5(b) and (c). The increased UPS and lower residual strain in the optimized heat-treated sample are attributed to the nano-grain microstructure resulting from the optimized heat treatment. Previous studies (Ref 17, 21) report similar trend for the influence of grain size on the UPS in binary NiTi. The increase in martensite onset yield strength, with decreasing grain size, following the Hall-Petch relation, minimizes the accumulation of the residual plastic strain arising from the stress-induced martensitic phase transformation.

**3.3.1 Uniaxial Tensile Test.** The addition of Co to NiTi changes the functional property of the NiTiCo vis-à-vis binary NiTi. For instance, (i) the phase transformation temperatures are lowered and (ii) the stiffness is increased. Before proceeding further, it is important to understand the definition of the term "stiffness" in regard to shape memory alloys. The term stiffness is closely associated with the elastic modulus. However, in the context of shape memory alloys, stiffness also implies the UPS. The modulus of elasticity is a fundamental property and is solely influenced by the interatomic bonding. In conventional alloys, thermo-mechanical treatments or alloying have minimal influence on this property because crystal structures remain the same (Ref 22). In shape memory alloys, thermo-mechanical treatments can be used to stabilize different phase(s) with different crystal structures at ambient temperature and can thus affect the elastic modulus at the ambient temperature. For example, R-phase or B19′ phase may be present at ambient temperatures depending on thermo-mechanical history. The UPS can be influenced by microstructural features such as precipitates, dislocations, and ternary additions—such as Co. In industry parlance, the NiTiCo alloys are typically referred to as high stiffness alloys. This implies that the NiTiCo alloy has
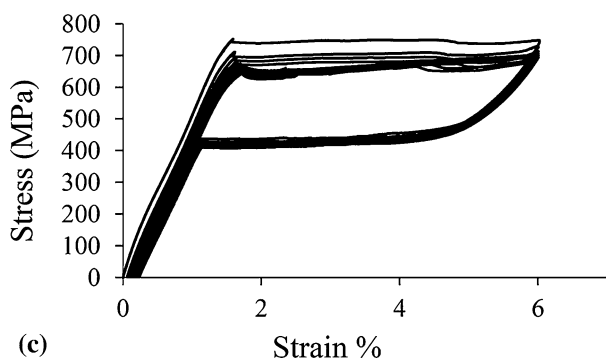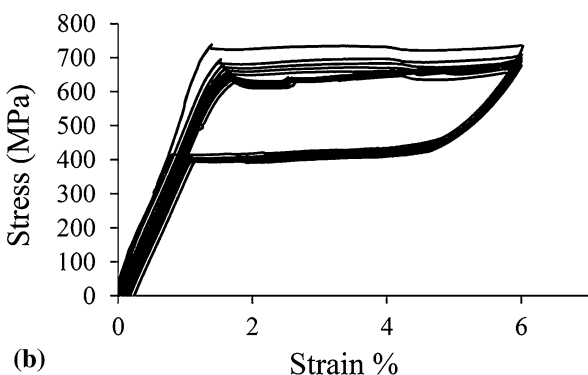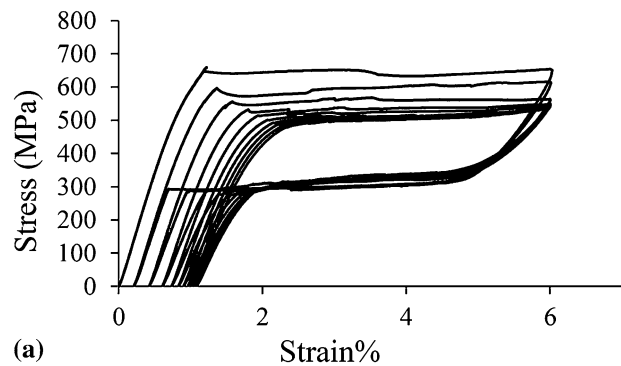
**(a)**



**(b)**



**(c)**

**Fig. 5** Cyclic stress-strain response of 0.5-mm NiTiCo wires processed at (a) 525 °C for 3.5 min, (b) 450 °C for 3.5 min, and (c) 450 °C for 5 min. The results show a stable upper plateau stress (UPS) and minimum residual strain for the alloy heat treated at 450 °C for 3.5 min



**(a)**



**(b)**

**Fig. 6** A comparison of the uniaxial tensile stress-strain response from (a) ternary NiTiCo and (b) binary NiTi. The results are from 0.5-mm-diameter re-drawn wires shape set at 525 °C for 3.5 min. The tests were carried at 20 °C above the active $A_f$, for the respective wires. NiTiCo has a higher upper plateau stress (UPS) than binary NiTi

**3.3.2 Rotary Beam Fatigue Test.** In high-quality NiTi and NiTi-based alloys, fatigue life is predominantly influenced by the maximum inclusion size (Ref 23, 24). This is due to the stress concentration at the inclusion-matrix interface. Recent studies have emphasized the importance of these interfaces toward fatigue life. For instance, Rahim et al. (Ref 24) elucidate the importance of particle-void assemblies (PVA's) between inclusions and matrix. They claim that the fatigue cracks preferentially nucleate at the PVA's, in the absence of surface defects. However, there are other factors such as thermo-mechanical treatments, surface finish, austenite finish ($A_f$) temperature, test temperature, test parameters, etc., that additionally influence the fatigue results (Ref 25). Hence, it is of utmost importance to maintain identical conditions to obtain fair and reproducible fatigue comparisons. For materials other than NiTi, a Stress-Life (S-N) fatigue curve is used to evaluate the material. When evaluating the fatigue life of NiTi, a Strain-Life (ε-N) curve is typically used. The reason for this difference is not merely because NiTi is prominent in the medical device industry and many medical devices are designed on strain-based parameters. Rather, the pseudoelastic upper plateau region of NiTi, where the stress in the material does not change with increasing strain, gives the S-N curve an almost unusable shape for product design and life prediction. Unfortunately, using a ε-N curve does not provide us with all the relevant information needed for a robust and thorough product design. The problem occurs when comparing materials with different stiffnesses. Figure 7 and 8 show RBT curves generated for

higher UPS than binary NiTi alloys. Figure 6 shows a representative stress-strain response of a binary NiTi and ternary NiTiCo shape memory alloy, processed under similar conditions. The samples were tested at 20 °C above the active $A_f$. The UPS, measured from Fig. 6, for NiTiCo and NiTi are 640 and 483 MPa, respectively. The UPS for the optimized NiTiCo, from Fig. 5, is 758 MPa. The relatively higher UPS in NiTiCo is attributed to (i) the Co addition and/or (ii) the thermo-mechanical treatment. Previous studies in NiTi and NiTi-based alloys have shown that by tailoring the thermo-mechanical treatment, the UPS can be adjusted (Ref 2). The TEM studies on optimized NiTiCo did not show Ni-rich precipitates. Hence, the higher UPS is attributed to the ternary Co addition and/or the nano-grain microstructure.
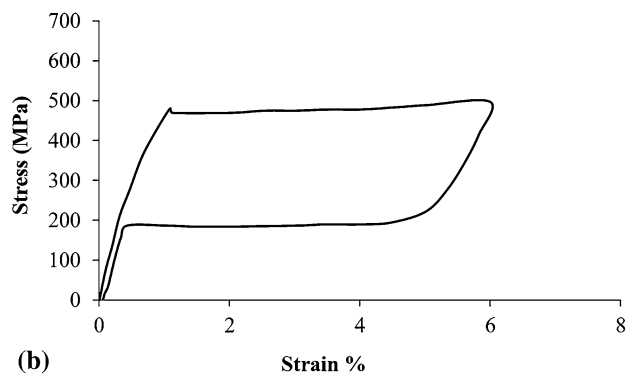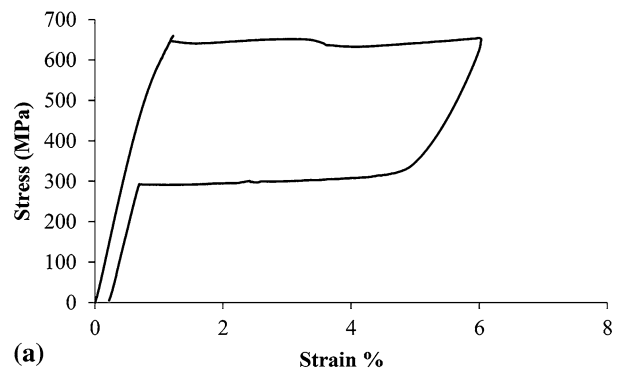
standard processed binary NiTi and optimally processed NiTiCo. Each point represents the average from 5 to 10 test samples. The fatigue samples in this study were tested at 37 °C. The details of the test set-up and test conditions are elaborated in (Ref 15). Figure 7 shows a typical ε-N comparison which suggests that NiTi has a similar run-out as NiTiCo at low strains but is slightly better in fatigue in the higher strain regions. When the same data are plotted as an S-N curve in Fig. 8, the NiTiCo is superior to NiTi in all regions of the curve. The data for stress in Fig. 8 are obtained from the uniaxial tensile stress-strain response by measuring the stress at the select strain.
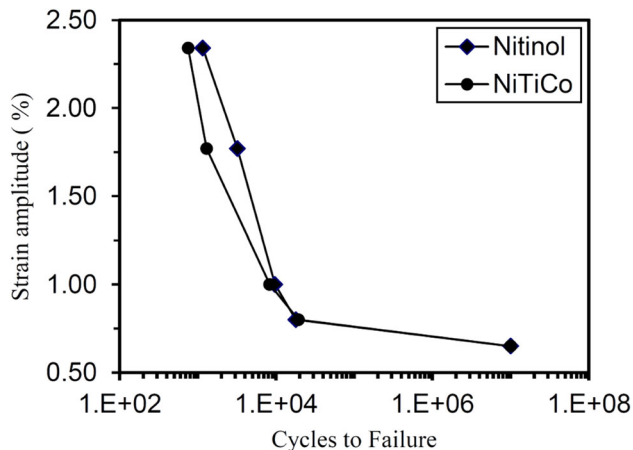


**Fig. 7** Fatigue test results obtained from rotating beam fatigue testing for NiTi and NiTiCo. The results show that NiTi performs better than NiTiCo at low-cycle fatigue. However, under high-cycle fatigue conditions, NiTi and NiTiCo have similar run-out
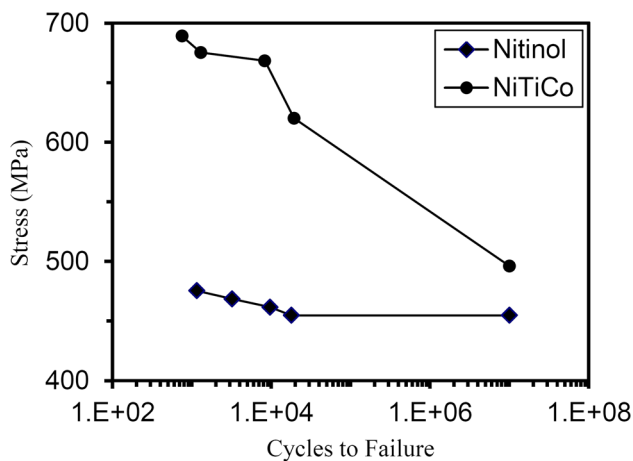


**Fig. 8** S-N curve for the data plotted in Fig. 7. The results show that for similar strain levels, NiTiCo generates higher stress levels, relative to NiTi

**Table 1  Comparison of stress levels at 0.5 and 1% strain in binary NiTi and ternary NiTiCo**

| Sample | Stress at 0.5% strain, MPa | Stress at 1% strain, MPa |
|---|---|---|
| NiTiCo | 517 | 758 |
| NiTi | 310 | 483 |

Strictly speaking, the test conditions are very different between the uniaxial tensile testing and the rotating beam fatigue testing and so the stress generated at a given strain will also differ between the two methods. However, the objective of showing Fig. 8, in the present work, is to emphasize that NiTiCo is a stiffer alloy than NiTi and under any test condition NiTiCo is expected to generate higher stress than NiTi, for a given strain. Figure 6 and Table 1 depict these differences. The stress at 0.5% strain in NiTi and NiTiCo are 310 and 517 MPa, respectively. Similarly, the stress at 1.0% strain for NiTi and NiTiCo are 483 and 758 MPa, respectively. A higher stress level at fixed strain will result in poor fatigue life. This is because, the interface between inclusions and the matrix are ideal for fatigue crack initiation (Ref 24, 26) and under identical conditions, the material with higher stress is bound to experience more damage at the interface and hence poorer fatigue. Thus, under similar strain level, one would expect the fatigue life of NiTiCo to be inferior to binary NiTi. This is what is observed in the low-cycle fatigue regime. However, in the high-cycle fatigue regime, where the wires were tested at strain amplitudes of 0.65 and 0.80%, NiTiCo exhibits comparable fatigue response to NiTi, despite the higher level of stress. This is because the NiTiCo system is either (i) in the elastic region or (ii) may have a mixture of austenite and R-phase, as opposed to binary NiTi which may have undergone some transformation to B19′ martensite. Thus, the fatigue life of NiTi will be influenced by—(i) inclusion-matrix interface and (ii) austenite-martensite interface, while that of NiTiCo will be only subject to the inclusion-matrix interface and hence lesser damage. The above statement is made with the assumption that the inclusion size and area fraction are comparable between the two alloys. Miyazaki et al. (Ref 27) have shown that the accumulation of plastic strain during mechanical cycling, in a uniaxial tensile set-up, is a result of the stress-induced martensitic phase transformation. Dislocations are generated at the austenite-martensite interface and result in the accumulation of plastic strain. The results from this work show that in addition to the austenite-martensite interface, the inclusion-matrix interface is also equally important. From a design perspective, a smaller diameter wire with a higher stiffness will develop less strain when bending and can still provide equivalent angular motion and compliance force in the device.

## 4. Conclusions

The objective of the current work was to understand the processing-structure-property correlation in a VIM-VAR-melted NiTiCo ternary shape memory alloy. To this end, microstructural, thermal, and mechanical characterization studies were carried on a thermo-mechanically processed NiTiCo alloy. Further, the fatigue properties of the ternary NiTiCo and binary NiTi were compared in rotating beam fatigue test. The major conclusions from this work are summarized below:

- Thermo-mechanical processing of NiTiCo alloys result in higher austenite start ($A_s$) temperature. The DSC results from the 0.53-mm re-drawn wire shows an $A_s$ of −2 °C, while the $A_s$ of a fully annealed coil is −73 °C. This is attributed to the optimized thermo-mechanical treatment, which suppresses the B19′ phase and introduces the R-phase transformation.

- The optimized heat treatment results in a nano-grain microstructure, which (i) suppresses the thermally induced B19′ phase transformation, (ii) introduces the R-phase transformation, (iii) inhibits the formation of Ni-rich precipitates, and (iv) enhances the superelastic response by improving the stability and minimizing the residual strain.
- The RBT results show that, the fatigue properties of NiTiCo are equivalent to that of binary NiTi. In making this comparison, it is important to account for the variation in the onset stress between the alloys. This is because, the stresses developed at similar strain levels are significantly different and influence the fatigue test results. Further studies with non-zero mean strain and stress conditions, which replicate the real working conditions would provide us with a better understanding of the fatigue properties of NiTiCo alloy.
- The benefit of using ternary NiTiCo stems from the advantage of obtaining higher stress at similar strain levels compared to binary NiTi. This will permit the design of device with smaller diameters or section thicknesses while retaining or improving functional properties.

## Acknowledgment

## References

1. H. Hosoda, S. Hanada, K. Inoue, T. Fukui, Y. Mishima, and T. Suzuki, Martensite Transformation Temperatures and Mechanical Properties of Ternary NiTi Alloys with off Stoichiometric Compositions, *Intermetallics*, 1998, **6**, p 291–301
2. K. Otsuka and X. Ren, Physical Metallurgy of Ti-Ni Based Shape Memory Alloys, *Prog. Mater. Sci*, 2005, **50**, p 511–678
3. Y. Nakata, T. Tadaki, and K. Shimizu, Atom Location of the Third Element in Ti-Ni-X Shape Memory Alloys Determined by the Electron Channeling Enhanced Microanalysis, *Mater. Trans. JIM*, 1991, **32**, p 580–586
4. Y. Kishi, Z. Yajima, and K. Shimizu, Relation Between Tensile Deformation Behavior and Microstructure in a Ti-Ni-Co Shape Memory Alloy, *Mater. Trans.*, 2002, **43**, p 834–839
5. Y. Kishi, Z. Yajima, K. Shimizu, and K. Morii, Effects of Microstructure on Mechanical Fatigue Crack Growth Characteristics of a Ti-Ni-Co Shape Memory Alloy, *Mater. Sci. and Eng. A*, 1999, **273-275**, p 654–657
6. A. Fasching, D.W. Norwich, T. Geiser, and G.W. Paul, An Evaluation of NiTiCo Alloy and Its Suitability for Medical Device Application, *J. Mater. Eng. Perform.*, 2011, **20**, p 641–645
7. X. Huang, D.W. Norwich, and M. Ehrlinspiel, Corrosion Behavior of Ti-55Ni-1.2Co High Stiffness Shape Memory Alloys, *J. Mater. Eng. Perform.*, 2014, **23**, p 2630–2634
8. Z. Lekston, D. Stróż, and M. Jędrusik-Pawłowska, Structure and Properties of Cold-Worked and Annealed Ti-Ni-Co Shape Memory Wires Designed for Medical Application, *Solid State Phenom.*, 2010, **63**, p 118–122
9. E.S. Mohammad, F. Karimzadeh, and A. Kermanpur, Nanocrystallization of the $Ti_{50}Ni_{48}Co_2$ Shape Memory Alloy by Thermomechanical Treatment, *J. Mater. Eng. Perform.*, 2015, **24**, p 445–451
10. "Standard Specification for Wrought Nickel-Titanium Shape Memory Alloy for Medical Devices and Surgical Implants" F2063-12, *Annual Book of ASTM Standards*, Section 13, ASTM, 2013, p 946–951
11. "Standard Specification for Chemical Passivation Treatments for Stainless Steel Parts"A967, *Annual Book of ASTM Standards*, Section 13, ASTM, 2014
12. "Standard Test Method for Transformation Temperature of Nickel-Titanium Alloys by Thermal Analysis" F2004-05, *Annual Book of ASTM Standards*, Section 13, ASTM, 2013, p 870–873
13. "Standard Test Method for Determination of Transformation Temperature of Nickel-Titanium Shape Memory Alloys by Bend and Free Recovery" F2082-06, *Annual Book of ASTM Standards*, Section 13, ASTM, 2013, p 998–1004
14. "Standard Test Method for Tension Testing of Nickel-Titanium Superelastic Materials", F2516-14, *Annual Book of ASTM Standards*, Section 13, ASTM, 2014
15. D.W. Norwich, A Comparison of Zero Mean Strain Rotating Beam Fatigue Test Methods for Nitinol Wire, *J. Mater. Eng. Perform.*, 2014, **23**, p 2515–2522
16. T. Waitz, V. Kazykhanov, and H.P. Karnthaler, Martensitic Phase Transformation in Nanocrystlline NiTi Studied by TEM, *Acta Mater.*, 2004, **52**, p 137–147
17. A. Ahadi and Q.P. Sun, Stress Hysteresis and Temperature Dependence of Phase Transition Stress in Nanostructured NiTi—Effects of Grain Size, *App. Phys. Lett.*, 2013, **103**, p 021902
18. J. Pons, L. Jordan, J.P. Morniroli, and R. Portier, Study of Dislocations Generated by Thermal Cycling in Ni-Ti-Co Shape Memory Alloys, *J. De Physq. IV*, 1995, **5**(C2), p 293–298
19. E.A. Prokofiev, J.A. Burow, E.J. Payton, R. Zarnetta, J. Frenzel, D.V. Gunderov, R.Z. Valiev, and G. Eggeler, Suppression of $Ni_4Ti_3$ Precipitation by Grain Size Refinement in Ni-rich NiTi Shape Memory Alloys, *Adv. Engg. Mater.*, 2010, **8**, p 747–753
20. M. Frotscher, P. Nörtershäuser, Ch. Somsen, K. Neuking, R. Böckmann, and G. Eggeler, Microstructure and Structural Fatigue of Ultra-Fine Grained NiTi-Stents, *Mater. Sci. and Eng. A*, 2008, **503**(1), p 96–98
21. J.E. Schaffer, Structure-Property Relationships in Conventional and Nanocrystalline NiTi Intermetallic Alloy Wire, *J. Mater. Eng. Perform.*, 2009, **18**, p 582–587
22. G.E. Deiter, *Mechanical Metallurgy*, McGraw-Hill Book Company, London, 1988
23. P.K. Kumar and C. Lasley, The Influence of Microcleanliness on the Fatigue Performance of Nitinol, *J. Mater. Eng. Perform.*, 2014, **23**(7), p 2457–2463
24. M. Rahim, J. Frenzel, M. Frotscher, J. Pfetzing-Micklich, R. Steegmüller, M. Wohlschlögel, M. Mughrabi, and G. Eggeler, Impurity Levels and Fatigue Lives of Pseudoelastic NiTi Shape Memory Alloys, *Acta Mater.*, 2013, **61**(10), p3667–3686
25. A. Pelton, J. DiCello and S. Miyazaki, Optimization of Processing and Properties of Medical-Grade Nitinol Wire, *Proceedings of the International Conference on Shape Memory and Superelastic Technologies* Eds., S.M. Russel and A.R. Pelton, Pacific Grove: International Organization on SMST, 2001, p 361–374
26. A. Toro, F. Zhou, M.H. Wu, W.V. Geertruyden, and W.Z. Misiolek, Characterization of Non-metallic Inclusions in Superelastic NiTi Tubes, *J. Mater. Eng. Perform.*, 2009, **18**, p 448–458
27. S. Miyazaki, T. Imai, Y. Igo, and K. Otsuka, Effect of Cyclic Deformation on the Pseudoelasticity Characteristics of Ti-Ni Alloys, *Met. Trans.*, 1986, **17**(1), p 115–120